iScience

CellPress
OPEN ACCESS

Article

Shared insights for heat health risk adaptation in metropolitan areas of developing countries

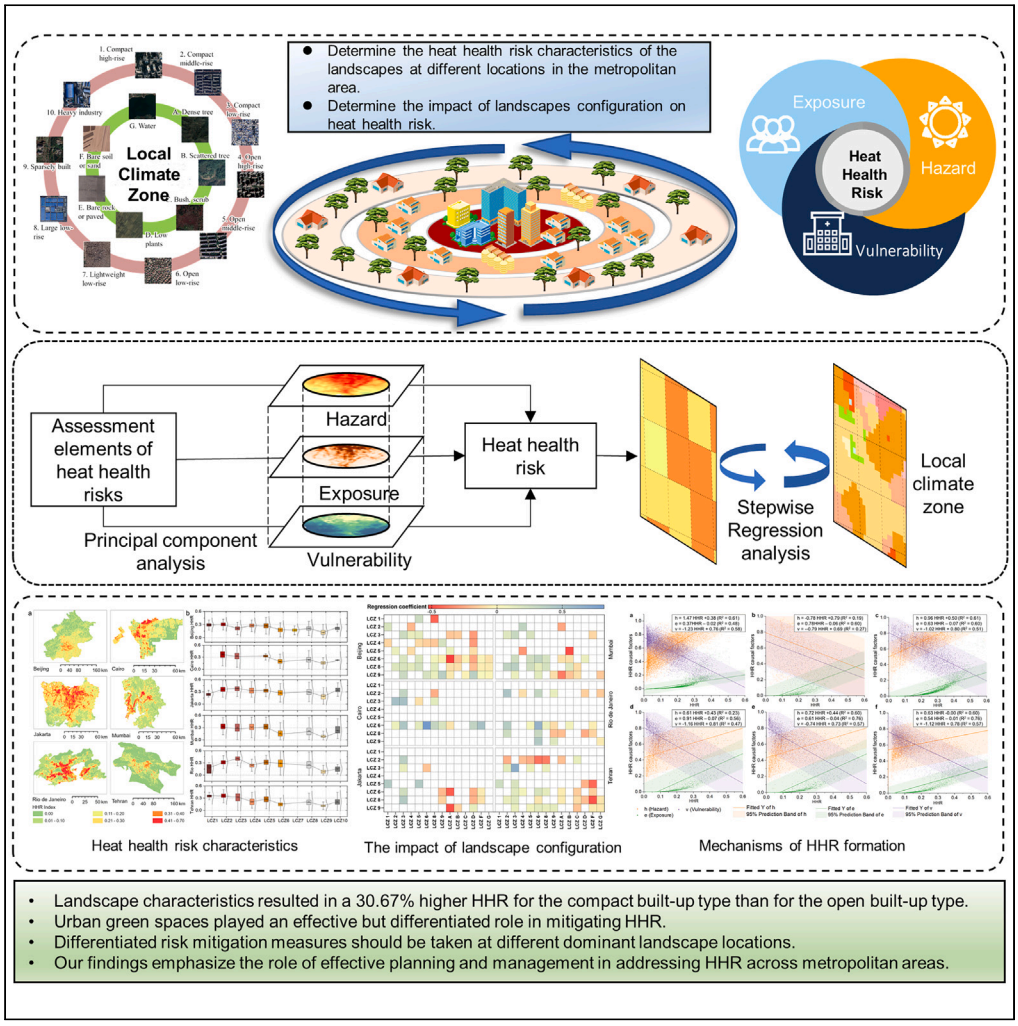

Wenbo Yu, Jun Yang, Dongqi Sun, ..., Xiangming Xiao, Jianhong(Cecilia) Xia, Xueming Li

yangjun8@mail.neu.edu.cn (J.Y.)
sundq@igsnrr.ac.cn (D.S.)

Highlights

The impact of the local landscape composition on heat health risk (HHR) is explored

Summarizes common and differential characteristic of HHR in different regions

Denser buildings are the most important cause of increased HHR

Urban green spaces play an effective but differentiated role in mitigating HHR

Yu et al., iScience 27, 109728
May 17, 2024
https://doi.org/10.1016/j.isci.2024.109728

iScience

CellPress
OPEN ACCESS

Article

Shared insights for heat health risk adaptation in metropolitan areas of developing countries

Wenbo Yu,[1,2] Jun Yang,[1,2,3,9,*] Dongqi Sun,[4,*] Bing Xue,[5] Wei Sun,[6] Jiayi Ren,[1] Huisheng Yu,[1] Xiangming Xiao,[7] Jianhong(Cecilia) Xia,[8] and Xueming Li[2]

SUMMARY

Global warming has led to a surge in heat health risks (HHRs), the impacts of which are particularly pronounced in metropolitan areas of developing countries. In the current study, six metropolitan areas - Beijing, China; Cairo, Egypt; Jakarta, Indonesia; Mumbai, India; Rio de Janeiro, Brazil; and Tehran, Iran - were selected as the study area to further differentiate the built-up landscapes by utilizing the concept of local climate zones. Moreover, we assessed the similarities and differences in HHR associated with the landscape. Results revealed a 30.67% higher HHR in compact built-up landscapes than in the open built-up type. Urban green spaces played an effective but differentiated role in mitigating HHR. That is, low vegetation in urbanized areas and trees in suburban areas significantly mitigated HHR. Collectively, our findings emphasize the role of effective planning and management in addressing HHR and provide empirical support for implementing HHR mitigation and adaptation strategies.

INTRODUCTION

Approximately 3.3–3.6 billion people worldwide inhabit highly climate-vulnerable environments.1 The Sixth Assessment Report of the Intergovernmental Panel on Climate Change (IPCC) predicts that global warming of $\geq 2^{\circ}C$ will increase the frequency with which extreme heat reaches critical tolerance thresholds for agricultural production and human health.[1] This will, in turn, increase the likelihood of climate-related health risks, such as heat stroke, dehydration, and cardiovascular disorders,[2,3] contributing to a rise in global mortality rates.[4–6] Reducing the risk of extreme heat in urban environments is also directly aligned with the objectives of sustainable development goal (SDG) 3 regarding good health and well-being, as well as SDG 11 which focuses on sustainable cities and communities.

Quantifying the impacts of climate change is a prerequisite for implementing remedial measures; the IPCC presented a risk-based framework for climate impact assessment in its Fifth and Sixth Assessment Reports.[7] In this framework, the risk is defined as the likelihood that climate will have adverse consequences for humans or ecosystems. Within this context, heat health risk (HHR) refers to the likelihood of adverse human health consequences from a hot environment. It is a function of hazard, exposure, and vulnerability that reflects the impact of high temperatures on human health. Moreover, HHR is consistent with the risk framework in the field of disaster risk reduction and management.[8] The urgency of addressing extreme HHR varies from global to national scales. On a global scale, areas with high HHRs are concentrated in underdeveloped or developing countries.[9,10] On a national scale, metropolitan areas emit large amounts of greenhouse gases,[11] and their large, continuous, impervious surfaces result in greater heat absorption,[12] leading to more severe thermal effects. Additionally, metropolitan areas face more complex urban development challenges than rural areas, often resulting in continuous urban sprawl,[13] dense urban populations,[14] and large socio-spatial inequalities,[15,16], particularly within underdeveloped and developing countries.[17,18] Hence, metropolitan areas experience greater HHRs as global urbanization intensifies.[19,20]

Although achieving global temperature control goals requires numerous countries to implement climate policies, increased HHRs are inevitable in hot environments owing to the trends in urban development and historical emissions.[21] Therefore, enhancing the capacity of vulnerable countries to adapt to climate change is particularly important for mitigating HHRs.[22] Due to the shared climate change challenges and similar cultural and social contexts present in developing countries, knowledge can be efficiently exchanged and solutions more rapidly

[1]School of Humanities and Law, Northeastern University, Shenyang 110169, China
[2]Human Settlements Research Center, Liaoning Normal University, Dalian 116029, China
[3]Jangho Architecture College, Northeastern University, Shenyang 110169, China
[4]Institute of Geographic Sciences and Natural Resources Research, Chinese Academy of Sciencess, Beijing 110016, China
[5]Institute of Applied Ecology, Chinese Academy of Sciences, Shenyang 110016, China
[6]Nanjing Institute of Geography and Limnology, Chinese Academy of Sciences, Nanjing 210008, China
[7]Department of Microbiology and Plant Biology, Center for Earth Observation and Modeling, University of Oklahoma, Norman, OK 73019, USA
[8]School of Earth and Planetary Sciences (EPS), Curtin University, Perth, WA 65630, Australia
[9]Lead contact
*Correspondence: yangjun8@mail.neu.edu.cn (J.Y.), sundq@igsnrr.ac.cn (D.S.)
https://doi.org/10.1016/j.isci.2024.109728

implemented. Under the Paris Agreement[23] and the Sustainable Development Goals,[24] most developing countries are preparing or have already issued national adaptation plans.[25] China has proposed a South–South cooperation, while a numerous African nations are working with the Global Center on Adaptation. However, cooperation in climate change adaptation is less common at the metropolitan scale.[20,26]

Spatial planning and management are crucial for HHR mitigation within metropolitan areas, focusing on urban population planning, natural and built landscapes, and the spatial layout of infrastructure[27,28] to reduce energy consumption and improve sustainability and adaptability.[29–31] To promote the exchange of relevant technologies and knowledge among vulnerable regions, the common and unique impacts of urban planning and management on HHR mitigation in metropolitan areas should be clarified. Local-scale HHRs vary based on the characteristics of the urban landscape, including the underlying surface type, which affects heat capacity, heat transfer, albedo, and anthropogenic heat emissions, resulting in varying heat hazards to humans.[32] Local residential and building attributes influence population distribution and outdoor heat exposure,[33] while also affecting poverty levels and access to healthcare resources.[18,34] Hence, comparing metropolitan areas vulnerable to HHRs from different countries within an administrative zoning scale is challenging. Thus, harmonized concepts must be introduced at the local scale as the basic unit for HHR management.[35–37]

The local climate zone (LCZ)[32] is a useful basic unit for local spatial planning and management, providing a refined description of the substrate and building characteristics within built-up areas. The LCZ is characterized by its "local scale," "climate nature," and "zoning properties." The local scale of LCZ is 10–1,000 m, which is finer than the administrative zoning scale. The "climate nature" of LCZ refers to the ten categories it is divided into according to the building structure and subsurface, making the urban heat island effect significant among different categories and better reflective of the dependence of the heat environment on the nature of the subsurface. The "zoning properties" of the LCZ refer to the relatively homogeneous building patterns in the same LCZ type; additionally, its description of the built-up area heights and densities can partially reflect the population density and socio-economic characteristics of the local population. Such information combined with local land functions and utilization patterns can be used to determine priority areas for spatial planning and management interventions.[38]

We examined six metropolitan areas in six developing countries—Beijing, Cairo, Jakarta, Mumbai, Rio de Janeiro, and Tehran—based on their size, continent, types of major buildings and natural landscapes, as well as political and economic status. Under the IPCC risk assessment framework, we locally assessed HHR using geospatial big data such as remote sensing, spatial location vectors, and downscaled statistical data. We analyzed the spatial distribution of HHR associated with LCZs in these metropolitan areas, considering both its level and causes. Furthermore, we clarified the potential effect of LCZ composition on HHR in urban, suburban, and fringe areas, identifying common denominators in using spatial planning tools to mitigate HHR.[39,40]

Overall, the purpose of this study is to test the ability of LCZ to distinguish HHR differences among global metropolitan areas and to summarise the commonalities and differences in LCZ-based HHR mitigation across metropolitan areas, which is quite different from previous HHR studies based on administrative units.[19,26,40] We used the LCZ concept to analyze the impact of landscape configuration, deriving intuitive and generalized conclusions to support the use of spatial planning and management tools for HHR mitigation. We highlighted commonalities in climate change responses among developing countries, offering effective mitigation strategies that are adaptable worldwide.

RESULTS

Heat health risks of compact landscapes and urban sub-centers

The spatial distribution of the HHR index and the HHR index of the built-up LCZs are shown in Figure 1. See Table S1 for detailed classification criteria for LCZ. High and sub-high HHR index levels were located primarily in urbanized areas. Compact-built landscapes (tightly packed with little to no green space) typically had higher HHRs than open-built landscapes (openly arranged buildings with an abundance of trees and a pervious cover) of the same height. This suggests that building density may be a common factor in HHR management. That is due to the higher subsurface permeability of open-type built-up landscapes and the abundance of shade produced by vegetation, particularly trees. Specifically, artificial shadows from vertical buildings and green spaces help minimize solar radiation absorption by open surfaces. Furthermore, the built landscapes of Jakarta and Rio de Janeiro had higher average HHR indexes, with the highest level continuously associated with compact low-rise landscapes. Beijing, Cairo, and Tehran also had widespread HHR distributions but at lower risk levels than those of Jakarta and Rio de Janeiro. Mumbai showed a linear clustered distribution of high HHR levels, with the lowest mean observed in built-up areas. Moreover, in Jakarta and Rio de Janeiro, the order of HHR index ranking was compact low-rise > compact mid-rise > compact high-rise, while in Beijing, Cairo, Mumbai, and Tehran, it was compact mid-rise > compact high-rise > compact low-rise. This further reflects the strong relationship between high HHR levels and the population's spatial distribution.

High-rise buildings in Rio de Janeiro and Jakarta were primarily located in the central business districts, with lower HHR indexes owing to smaller populations and public green spaces in the surrounding areas, highlighting a potential mismatch between land development intensity and population exposure.

The top 1% of HHRs, indicating extreme heat, were observed in specific regions (Figure 2). In Cairo, Jakarta, Mumbai, Tehran, and Rio de Janeiro, extreme HHRs exhibited a doughnut-shaped effect, with central areas experiencing lower impacts and surrounding sub-centers being affected to a higher degree. This highlights the importance of monitoring and responding to HHRs in metropolitan sub-centers.

In Central Jakarta, extreme HHRs were rare, primarily occurring in Tangerang, Debo, and Bekasi (regions immediately surrounding Central Jakarta) and their surrounding areas. Conversely, Beijing saw spillover effects of extreme HHRs, with metropolitan area centers affected to a higher degree and metropolitan sub-centers to a lower degree. More specifically, the extreme HHRs had a large, continuous distribution in the central area and a small, concentrated distribution in the sub-central areas, such as Changping and Tongzhou.

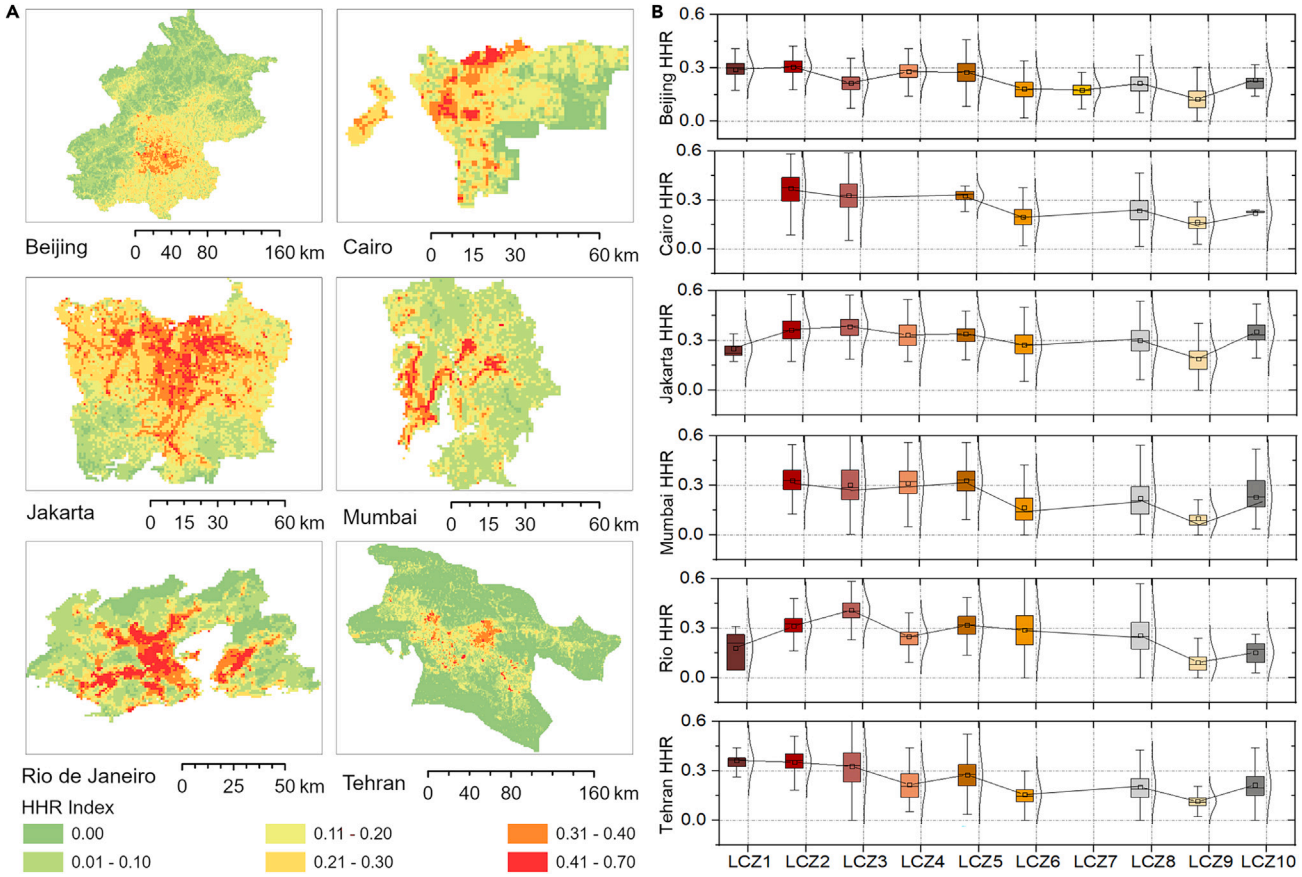

Figure 1. Spatial distribution of HHR index and the HHR index of built-up type LCZs

(A) Spatial distribution of the HHR index. The normalized hazard, exposure, and vulnerability were developed using the multiplication principle to express the HHR index (ranging from 0 to 1). The closer the color is to red, the higher the potential impact from HHR. The ranking order of the HHR index for built-up areas is as follows: Rio de Janeiro (0.282)>Jakarta (0.279)>Cairo (0.258)>Tehran (0.216)>Beijing (0.197)>Mumbai (0.185).

(B) HHR index of built-up LCZs. Definition of LCZ: LCZ 1–3 for compact high, middle and low–rise built types, LCZ 4–6 for open high, middle, low-rise built types, LCZ 7 for light low–rise built type, LCZ 8 for large low-rise built type, LCZ 9 for sparsely built type, LCZ 10 for heavy industry, The mean HHR of the compact built type (0.326) > open built type (0.226) > sparsely built type (0.131). The boxes indicate the range of data distribution from 25% to 75%, the horizontal lines and dots in the boxes indicate the median and mean, respectively, and the whiskers indicate the range within 1.5 times the interquartile range.

Changes in the hierarchy of heat health risk types in relation to the landscape

The spatial distribution of HHR types in the six metropolitan areas and their LCZ characteristics are shown in Figure 3. The HHR types primarily exhibited a hierarchical pattern with a clustered distribution, transitioning gradually from urbanized to peripheral areas. Owing to differences in the peripheral natural landscape, urbanized metropolitan areas in Beijing, Jakarta, Mumbai, and Rio de Janeiro were categorized as Hh-Lv-He (LCZ A/B with dense and scattered trees in the peripheral landscape), whereas those in the urbanized Cairo and Tehran metropolitan areas were Lh-Lv-He (LCZ F with bare ground in the peripheral landscape). The regions outside the urbanized areas ranged from the Hh-Lv-Le to Hh-Hv-Le types and then to the Lh-Hv-Le type.

Notably, despite lower heat hazards in urban Cairo and Tehran compared to the extremely high temperatures in peripheral bare soil areas, these urban regions exhibited high surface temperatures. Therefore, although these areas were classified as low-hazard areas based on the HHR type, they exhibited a high potential heat hazard.

Similarities and differences were observed in the types of HHR-specific causal factors between landscapes in different metropolitan areas. We focused on areas affected by multiple HHR causal factors. The commonality was reflected by the compact built-type landscapes being more affected by dual HHR-specific causal factors than open landscapes. The dominant landscapes LCZ 1–5 in urbanized areas were affected primarily by high heat hazards and exposure, whereas the dominant landscapes LCZ 6, 8, and 9 in suburban and peripheral areas were affected by high heat hazard and vulnerability. These differences arose from the effects of high exposure on different LCZ types across metropolitan areas. High heat exposure was concentrated in high-rise landscapes in Beijing, mid-rise landscapes in Cairo, Jakarta, and Mumbai, and low-rise landscapes in Rio de Janeiro. Suburban and peripheral metropolitan areas have complex and variable HHR-specific causal factors, usually a combination of different HHR types. In all metropolitan areas, a small portion of LCZ 3 compact low-rise, LCZ 6 open low-rise,

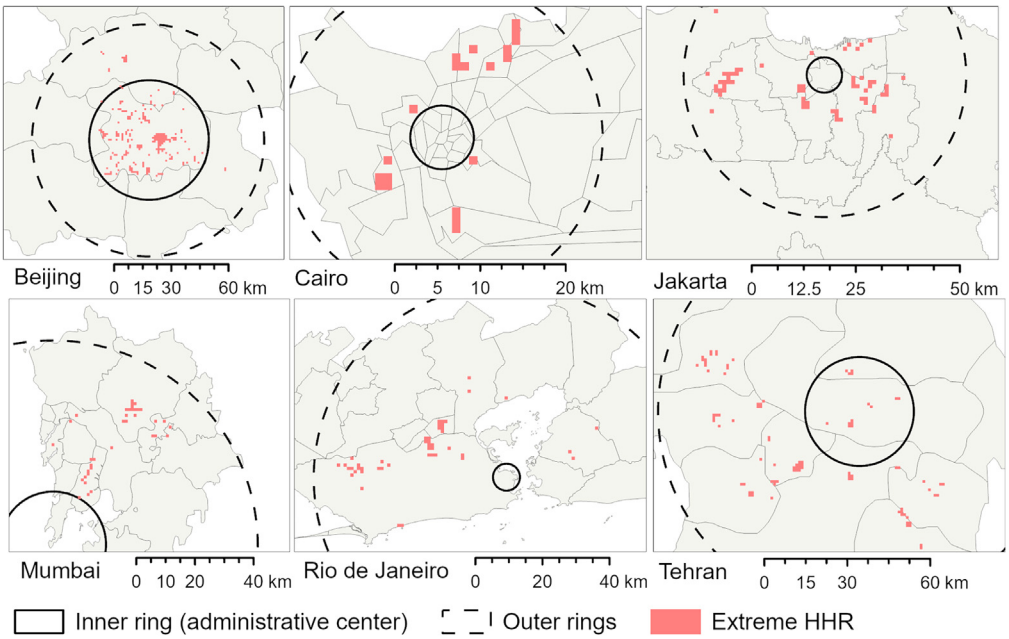

Figure 2. Doughnut and spillover effects of extreme HHRs

The highest 1% of HHRs in the grid were observed for extreme heat experiencing regions. The inner ring represents the approximate boundary of the administrative center of the metropolitan area, and the outer ring represents the approximate boundary of the extreme HHR distribution. In Beijing, extreme HHRs had spillover effects, with metropolitan area centers and sub-centers being affected to a higher and a lower degree, respectively. In other metropolitan areas, extreme HHRs produced a doughnut effect, where the center and surrounding sub-centers of the metropolitan area were affected to a lower and a higher degree, respectively.

and LCZ 8 large low-rise areas had the most high-risk regions, with three HHR-specific causal factors. In Mumbai, LCZ 6 and 9 primarily comprised two diametrically opposed types (Hh-Hv-Le and Lh-Lv-He), reflecting a highly complex risk management profile.

Suburban and peripheral areas of Cairo and Tehran had higher percentages of high heat hazards than urbanized areas. Insufficient social and physical infrastructure designed to mitigate the effects of extreme heat causes disproportionate exposure and impacts the most vulnerable populations. This ultimately leads to higher mortality rates, emphasizing the importance of effective cooling measures in these areas.

Mitigation options based on heat health risk driving mechanisms

We further analyzed the correlation between the HHR index and its causal factors (Figure 4) and observed similarities in the mechanisms underlying HHRs across different metropolitan areas. Notably, all locations exhibited a high level of heat hazard. Heat vulnerability and exposure were the primary risk factors in low- and high-HHR areas, respectively.

Nevertheless, the mechanisms underlying HHR varied across the different metropolitan areas. Heat hazards were weakly correlated ($R^2 < 0.3$) with HHR levels in Cairo and Tehran, where LCZ F bare soil was the main natural landscape. In metropolitan areas where LCZ A dense trees were the main natural landscape, HHR levels were positively correlated with heat hazards. Linear regression analysis revealed that HHR sensitivity to heat exposure variations was higher in Beijing, Jakarta, and Tehran, while Mumbai was primarily sensitive to changes in heat hazard. In Cairo and Rio de Janeiro, the HHR was sensitive to heat hazard and exposure. Therefore, metropolitan areas should adopt differentiated HHR mitigation strategies based on their sensitivity to specific risk factors.

Urban green offers an effective and differentiated role in mitigation

We assessed the effect of built-up landscapes on HHR, designating the local major landscape as that with the highest percentage within the grid. Based on the differences in local major landscapes, the heterogeneous effects of LCZ composition on HHR in urbanized areas (local major landscapes LCZs 1–5) as well as suburban and peripheral areas (locally major landscapes LCZs 6,8,9) were analyzed separately; the results are presented in Table S2.

LCZ 6 open low-rise and LCZ 8 large low-rise primarily served to mitigate HHR in urbanized areas while increasing it in suburban areas. Natural-type LCZs consistently mitigated HHR in urbanized and suburban areas, with LCZ D low vegetation having a more pronounced impact in urbanized areas. In the urbanized area of Beijing, the mitigation effect of low vegetation was 3.69 times greater than that of trees. In the urbanized areas of Cairo, Mumbai, Rio de Janeiro, and Tehran, mitigating effects were only observed for low vegetation, while LCZ A dense trees played a notably larger mitigating role in suburban areas. Although LCZ G water bodies individually posed a low heat hazard, their interaction with built-up-type LCZs was minimal. Consequently, their HHR mitigation effects were less pronounced than those of green spaces.

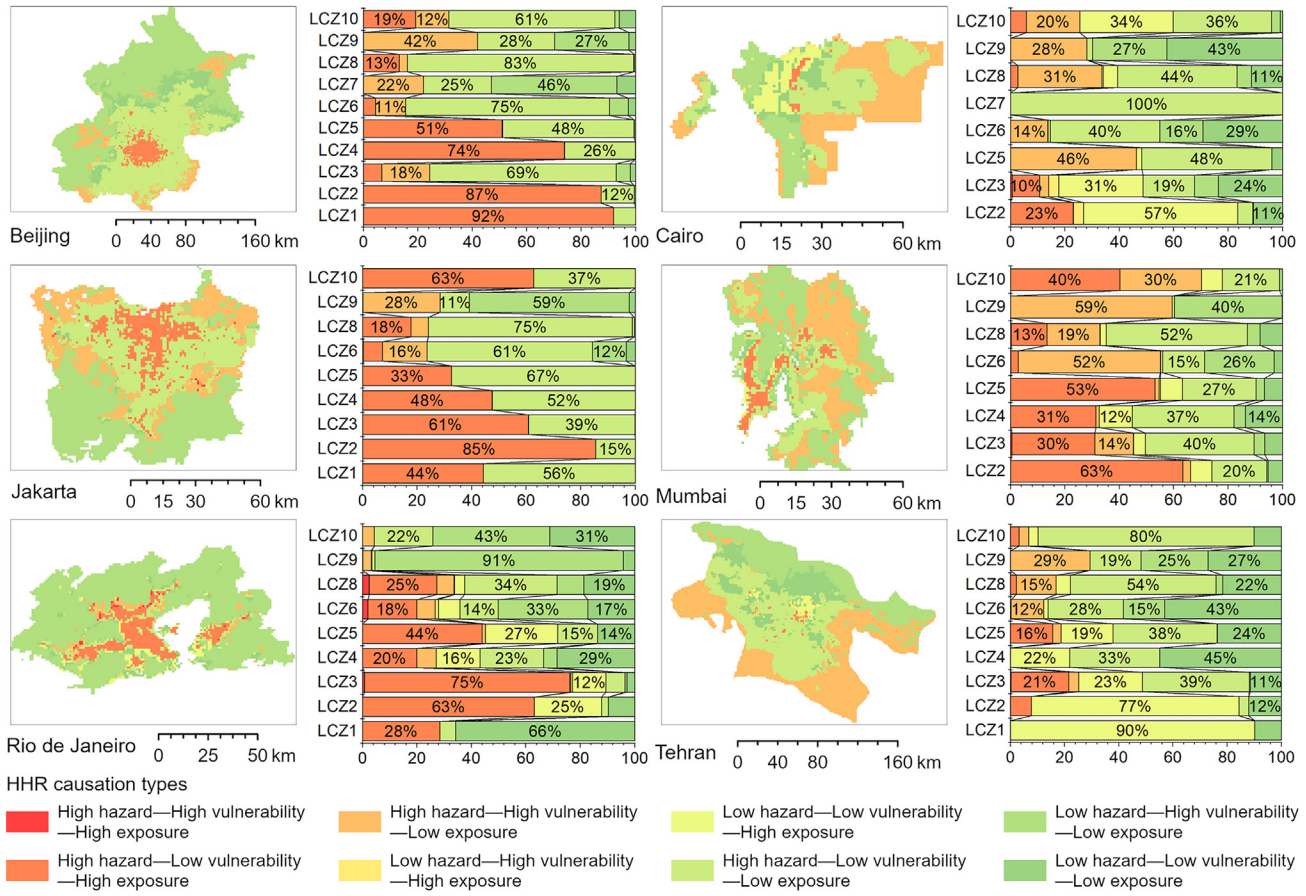

Figure 3. Spatial distribution of HHR types and characteristics of HHR types in the LCZ

The hazard degree (h), exposure degree (e), and vulnerability degree (v) of HHRs were classified into two categories, high (H) and low (L), according to the natural breakpoint method to classify the types of HHRs. The HHR types primarily showed a hierarchical change pattern with a clustered distribution and gradual change from urbanized to peripheral areas (Hh-Lv-He type or Lh-Lv-He type to Hh-Lv-Le type to Hh-Hv-Le type and then to Lh-Hv-Le type).

We further analyzed the effect of LCZ composition on HHR under each major built-type landscape (Figure 5). Mixing compact types LCZ 1, 2, and 3 further elevated the HHR index, whereas mixing open types LCZ 4 and 5 had a reducing effect. The HHR index of LCZ 6-dominated grids decreased with the addition of LCZs A–G. In grids dominated by LCZ 9 landscape, the HHR index decreased only when LCZ A/B dense or scattered trees were introduced. Conversely, the HHR index increased with the addition of other built or natural types of LCZs. This indicates that green spaces, such as low vegetation or shrubs, do not exert the same HHR mitigation effects in peripheral areas as in urbanized and suburban areas.

DISCUSSION

Planning- and management-based heat health risks mitigation strategies

We have identified potential solutions for adapting to changing heat environments and mitigating HHRs using local-scale planning and management based on the LCZ concept.[41] Our findings inform the expansion of South–South cooperation to promote climate change adaptation.[42] Herein, certain similarities were detected in how LCZ composition influences HHR across metropolitan areas, suggesting the potential for cooperation in planning and management among southern metropolitan areas. We also discovered that the effects of LCZ composition on HHR differ among urbanized, suburban, and peripheral areas, highlighting the need for tailored mitigation measures. The study areas and framework were summarized in Figure 6.

Regarding planning, nature-based solutions have received increasing international attention since the September 2019 UN Summit in New York,[43] which emphasized the important role of green spaces and infrastructure in urban climate regulation.[29–31,44] However, the Adaptation Gap report from 2020 revealed that only 13% of investments in the four major climate and development funds were allocated to nature-based climate risk solutions, and local-scale knowledge support was equally lacking.[45] Our findings confirm that green spaces effectively mitigate HHRs; however, their impact varies based on factors such as location, type of green space, or local environmental conditions. Therefore, adapted HHR mitigation measures are recommended for different LCZ locations in metropolitan areas.

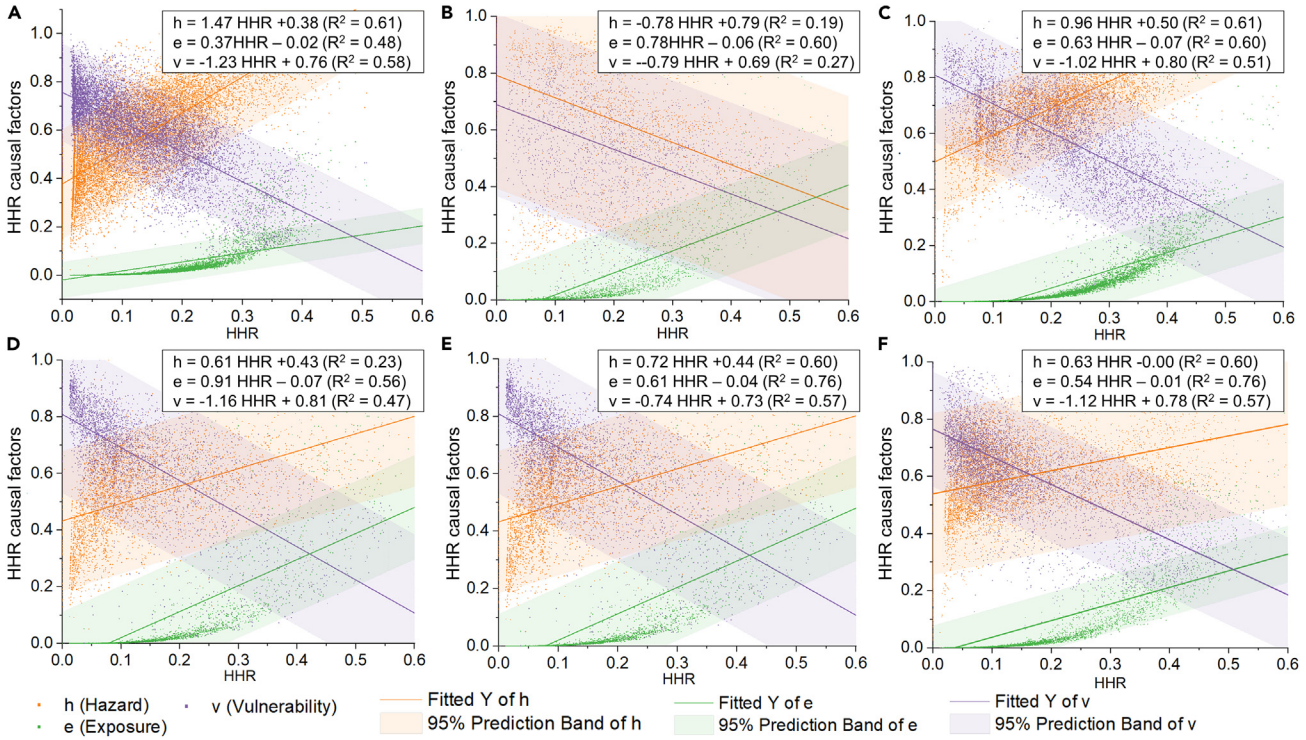

Figure 4. Effect of causal factors on HHR index

(A–F) show the linear relationship between HHR causal factors and HHR index in Beijing, Cairo, Jakarta, Mumbai, Rio de Janeiro, and Tehran, respectively. The horizontal axis represents the HHR index, and the vertical axis represents the three risk causal factors of hazard, exposure and vulnerability. Positive and negative slopes represent positive and negative correlations between HHR and causal factors, respectively. A smaller absolute value of the slope indicates that a change in the causal factor will have a greater impact on the HHR index.

LCZs 1–5 are located primarily in the core urban settings of metropolitan areas, i.e., the region with the highest population concentration and the most complete range of public services. This study demonstrated that the main characteristics of these LCZs are high risk, high exposure, and low vulnerability, and a high HHR. This supports our results, indicating that dense or scattered trees in LCZ A and B landscapes had a greater HHR reduction effect than in LCZ D low-vegetation landscape. However, in LCZs 1–5, the cooling effect of trees is not sufficiently appreciated when designing mitigation strategies. Other studies have also demonstrated that urban parks can elicit a significant cooling effect on the environment within a certain distance.[46–49] Therefore, metropolitan areas may consider mitigating the very high heat risk by allocating parkland to locations where it is concentrated. Moreover, considerable changes in landscape patterns may reduce population density and economic development in metropolitan areas.[37] In locations with set landscape patterns, open landscapes should be considered to amplify HHR mitigation. In such cases, transitioning from compact to open landscapes can be achieved by planting street trees or adding green facades and roofs.[50–52] Macroscopic planning for ventilation and ecological corridors can also have a cooling effect by improving the air circulation efficiency in high-density areas.[53,54] Meanwhile, to further mitigate their high heat exposure, metropolitan areas should also consider appropriately shifting the LCZ 1–5 portion of the population to lower heat risk locations.[55–61]

LCZ 6 is predominantly located in areas outside the urban core, a rapidly urbanizing zone immediately adjacent to the urban core that typically presents low heat exposure. Compared to LCZs 1–5, this area has lower heat hazard but higher heat vulnerability and lower overall heat risk. The results of our local landscape configuration analyses suggest that mixing LCZ 6 with LCZs 1–5 elevates its HHR while mixing with natural-type LCZs generally results in a decrease in HHR. As the area with the most frequent development activities in the metropolitan area, the addition of compact type landscapes to LCZ 6 can reasonably enhance the land use efficiency and the allocation of various public service infrastructures, such as parks, medical centers, and roads, to serve the population transferred from the LCZ 1–5 landscapes and achieve an overall reduced HHR in the metropolitan area.[62]

LCZ 9 is typically located in the fringe settlements of metropolitan areas, often characterized by low heat exposure and high heat vulnerability of the HHR type. Although these zones typically have the lowest heat hazard, the lack of adequate social and physical infrastructure capacity to cope with the impacts of extreme heat can result in greater heat risk than that in the core zones. This is particularly true for Cairo and Tehran, with higher heat hazards on the periphery of their metropolitan areas. The landscape configuration analyses suggested that LCZ A/B alone may reduce the heat hazard of LCZ 9. Consequently, a need exists to mitigate the potential HHR in these zones by reducing heat vulnerability. Specifically, the population can be concentrated by clustering high-quality facilities in relatively populous areas, expanding the population covered by public service facilities, and facilitating the adoption of policy measures to limit the metropolitan area sprawl.[63] In

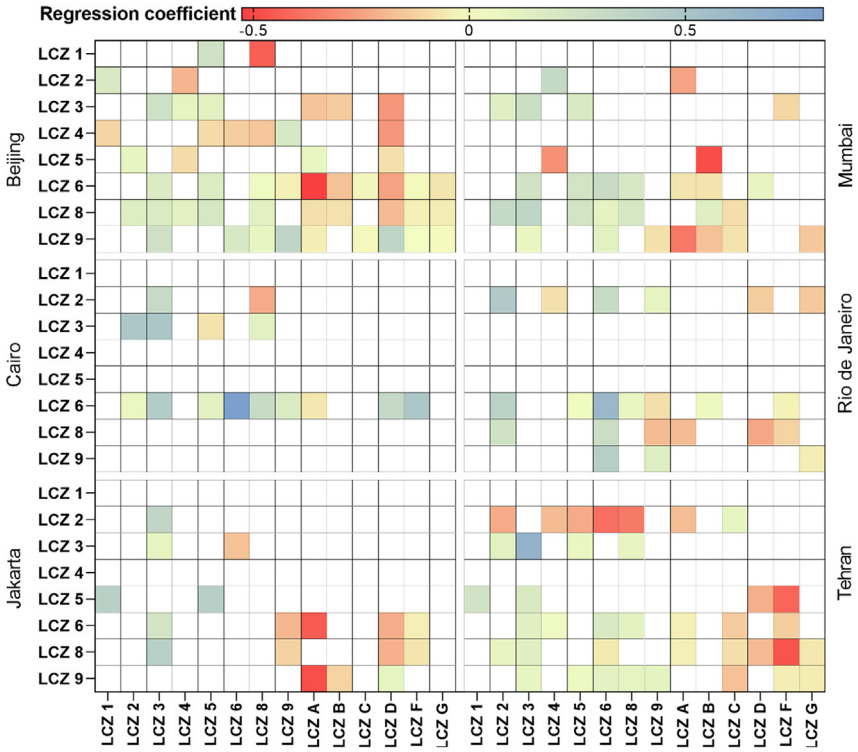

Figure 5. Regression coefficients of LCZ composition ratios for the different LCZ-dominant-type grids according to HHR level

Vertical for locally major built-up type LCZs and horizontal for minor type LCZs. Definition of LCZs: LCZ 1–3 for compact high-, middle-, and low-rise buildings; LCZ 4–6 for open high, middle, and low-rise buildings; LCZ 8 for large low-rise buildings; LCZ 9 for sparsely built type; LCZ A–B for dense and scattered trees; LCZ C for bush or scrub; LCZ D for low plants; LCZ E for bare rock; LCZ F for bare soil; LCZ G for water bodies. A smaller regression coefficient indicates a more pronounced HHR mitigation when a minor landscape is configured in the major landscape.

addition, the local governments should strengthen the dissemination of knowledge regarding heat wave risks and preventive measures while also providing basic livelihood protection, such as financial subsidies and cooling equipment (e.g., fans, air-conditioners) to vulnerable populations, including the elderly.[26]

Limitations of the study

Owing to computational limitations, only six key metropolitan areas in developing countries with different geographic subdivisions were selected for this study. Although our analysis broadly reflects the common characteristics of HHR in developing countries, we acknowledge that HHR varies significantly among metropolitan areas. Therefore, to more comprehensively explore the impacts of heat risk, subsequent studies should encompass additional metropolitan areas, particularly in underdeveloped countries that tend to be less equipped to handle heat-related changes. In addition, imaging HHR spatial divergence based on long-time series variation in the LCZ of a metropolitan area is an important research direction. However, the existing global LCZ maps only support studies from ~2020; hence, more in-depth analyses are necessary.

STAR★METHODS

Detailed methods are provided in the online version of this paper and include the following:

- KEY RESOURCES TABLE
- RESOURCE AVAILABILITY
  - Lead contact
  - Materials availability
  - Data and code availability
- EXPERIMENTAL MODEL AND STUDY PARTICIPANT DETAILS
- METHOD DETAILS
  - Study area

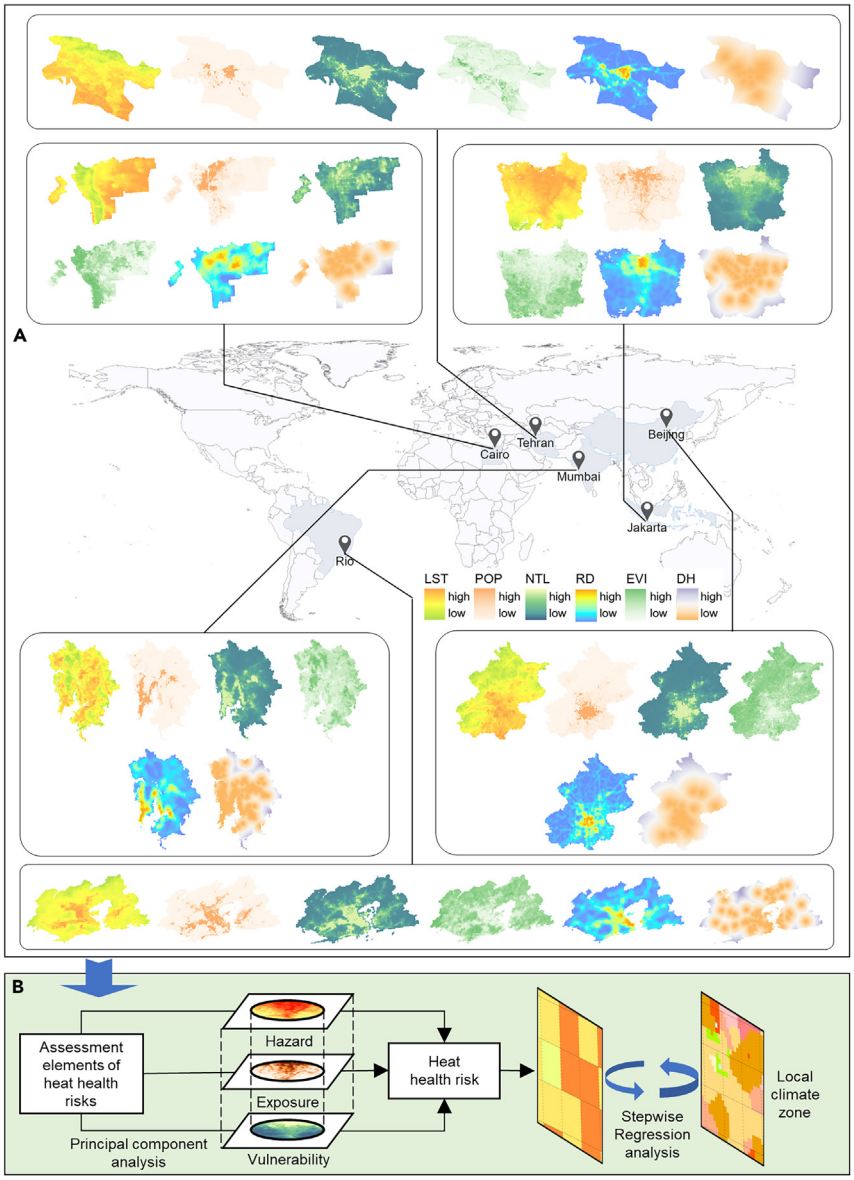

Figure 6. Overview of the study area and framework

(A) Location of the study area and spatial distribution of HHR assessment elements. The study area comprises Beijing, Cairo, Jakarta, Mumbai, Rio de Janeiro and Tehran metropolitan areas. LST: land surface temperature, POP: population, NTL: nighttime light index, RD: road network density, EVI: enhanced vegetation index, DH: distance to medical facilities.

(B) Exploring the effect of LCZ composition on HHR level using a stepwise linear regression model. Hazard was expressed in terms of land surface temperature, exposure was expressed in terms of population density, and vulnerability was synthesized using principal component analysis for nighttime lighting, road density, enhanced vegetation index, and distance from hospital.

SUPPLEMENTAL INFORMATION

Supplemental information can be found online at https://doi.org/10.1016/j.isci.2024.109728.

ACKNOWLEDGMENTS

This research study was supported by the National Natural Science Foundation of China (grant no's 41771178, 42030409, and 41671151), the Fundamental Research Funds for the Central Universities (grant no. N2411001), Basic Scientific Research Project (Key Project) of the Education Department of Liaoning Province (grant no. LJKZ0964), Natural Science Foundation of Guizhou Province (grant no. (2019)1150).

The authors would like to acknowledge all colleagues and friends who have voluntarily reviewed the translation of the survey and the article of this study. We would like to thank Gianvito Scaringi, editor of Editage (www.editage.cn), for his English-language editing.

AUTHOR CONTRIBUTIONS

Conceptualization, J.Y., B.X., and W.S.; methodology, J.R., H.Y.; formal analysis, W.Y.; data curation, W.Y..; writing – original draft, W.Y.; writing – review and editing, J.X., D.S.; supervision, X.L., X.X.

DECLARATION OF INTERESTS

This article has not been published or presented elsewhere in part or in entirety and is not under consideration by another journal. We have read and understood your journal's policies, and we believe that neither the article nor the study violates any of these. The authors declare no competing interests.

Received: October 27, 2023
Revised: March 2, 2024
Accepted: April 9, 2024
Published: April 12, 2024

REFERENCES

1. IPCC WGII (Intergovernmental Panel on Climate Change, Working Group II) (2022). AR6 Climate Change 2022: Impacts, Adaptation and Vulnerability. Climate Change 2022: Impacts, Adaptation and Vulnerability. https://www.ipcc.ch/report/ar6/wg2/.
2. IPCC (2015). Summary for Policymakers — Global Warming of 1.5 °C. https://www.ipcc.ch/sr15/chapter/spm/.
3. Welsby, D., Price, J., Pye, S., and Ekins, P. (2021). Unextractable fossil fuels in a 1.5 °C world. Nature *597*, 230–234. https://doi.org/10.1038/s41586-021-03821-8.
4. Ebi, K.L., Capon, A., Berry, P., Broderick, C., de Dear, R., Havenith, G., Honda, Y., Kovats, R.S., Ma, W., Malik, A., et al. (2021). Hot weather and heat extremes: health risks. Lancet *398*, 698–708. https://doi.org/10.1016/S0140-6736(21)01208-3.
5. Lee, W., Kim, Y., Sera, F., Gasparrini, A., Park, R., Michelle Choi, H., Prifti, K., Bell, M.L., Abrutzky, R., Guo, Y., et al. (2020). Projections of excess mortality related to diurnal temperature range under climate change scenarios: a multi-country modelling study. Lancet Planet. Health *4*, e512–e521. https://doi.org/10.1016/S2542-5196(20)30222-9.
6. Vanos, J.K., Baldwin, J.W., Jay, O., and Ebi, K.L. (2020). Simplicity lacks robustness when projecting heat-health outcomes in a changing climate. Nat. Commun. *11*, 6079. https://doi.org/10.1038/s41467-020-19994-1.
7. IPCC WGII (Intergovernmental Panel on Climate Change, Working Group II) (2014). AR5 Climate Change 2014: Impacts, Adaptation, and Vulnerability. https://www.ipcc.ch/report/ar5/wg2/.
8. UNISDR (2017). Words into Action guidelines: National disaster risk assessment. http://www.undrr.org/publication/words-action-guidelines-national-disaster-risk-assessment.
9. Dong, W., Liu, Z., Liao, H., Tang, Q., and Li, X. (2015). New climate and socio-economic scenarios for assessing global human health challenges due to heat risk. Climatic Change *130*, 505–518. https://doi.org/10.1007/s10584-015-1372-8.
10. Pal, J.S., and Eltahir, E.A.B. (2016). Future temperature in southwest Asia projected to exceed a threshold for human adaptability. Nat. Clim. Change *6*, 197–200. https://doi.org/10.1038/nclimate2833.
11. Muñiz, I., and Sánchez, V. (2018). Urban Spatial Form and Structure and Greenhouse-gas Emissions From Commuting in the Metropolitan Zone of Mexico Valley. Ecol. Econ. *147*, 353–364. https://doi.org/10.1016/j.ecolecon.2018.01.035.
12. Min, M., Lin, C., Duan, X., Jin, Z., and Zhang, L. (2019). Spatial distribution and driving force analysis of urban heat island effect based on raster data: A case study of the Nanjing metropolitan area, China. Sustain. Cities Soc. *50*, 101637. https://doi.org/10.1016/j.scs.2019.101637.
13. Novotný, J., Chakraborty, S., and Maity, I. (2022). Urban expansion of the 43 worlds' largest megacities: A search for unified macro-patterns. Habitat Int. *129*, 102676. https://doi.org/10.1016/j.habitatint.2022.102676.
14. Kii, M. (2021). Projecting future populations of urban agglomerations around the world and through the 21st century. npj Urban Sustain. *1*, 10. https://doi.org/10.1038/s42949-020-00007-5.
15. de Castro Mazarro, A., Sikder, S.K., and Pedro, A.A. (2022). Spatializing inequality across residential built-up types: A relational geography of urban density in São Paulo, Brazil. Habitat Int. *119*, 102472. https://doi.org/10.1016/j.habitatint.2021.102472.
16. Han, Y., He, J., Liu, D., Zhao, H., and Huang, J. (2023). Inequality in urban green provision: A comparative study of large cities throughout the world. Sustain. Cities Soc. *89*, 104229. https://doi.org/10.1016/j.scs.2022.104229.
17. Song, J., Huang, B., Kim, J.S., Wen, J., and Li, R. (2020). Fine-scale mapping of an evidence-based heat health risk index for high-density cities: Hong Kong as a case study. Sci. Total Environ. *718*, 137226. https://doi.org/10.1016/j.scitotenv.2020.137226.
18. Sun, Y., Li, Y., Ma, R., Gao, C., and Wu, Y. (2022). Mapping urban socio-economic vulnerability related to heat risk: A grid-based assessment framework by combing the geospatial big data. Urban Clim. *43*, 101169. https://doi.org/10.1016/j.uclim.2022.101169.
19. Estoque, R.C., Ooba, M., Seposo, X.T., Togawa, T., Hijioka, Y., Takahashi, K., and Nakamura, S. (2020). Heat health risk assessment in Philippine cities using remotely sensed data and social-ecological indicators. Nat. Commun. *11*, 1581. https://doi.org/10.1038/s41467-020-15218-8.
20. Aubrecht, C., and Özceylan, D. (2013). Identification of heat risk patterns in the U.S. National Capital Region by integrating heat stress and related vulnerability. Environ. Int. *56*, 65–77. https://doi.org/10.1016/j.envint.2013.03.005.
21. Roelfsema, M., van Soest, H.L., Harmsen, M., van Vuuren, D.P., Bertram, C., den Elzen, M., Höhne, N., Iacobuta, G., Krey, V., Kriegler, E., et al. (2020). Taking stock of national climate policies to evaluate implementation of the Paris Agreement. Nat. Commun. *11*, 2096. https://doi.org/10.1038/s41467-020-15414-6.
22. Shi, L., and Moser, S. (2021). Transformative climate adaptation in the United States: Trends and prospects. Science *372*, eabc8054. https://doi.org/10.1126/science.abc8054.
23. UNFCCC (2015). The Paris Agreement. https://unfccc.int/process-and-meetings/the-paris-agreement.
24. UNECE (2017). UNECE and the SDGs (UNECE). https://unece.org/unece-and-sdgs.
25. UNEP (2021). Strengthening climate adaptation, otherwise facing serious human and economic losses (UN Environment). http://www.unep.org/zh-hans/xinwenyuziyuan/xinwengao-24.
26. Dong, J., Peng, J., He, X., Corcoran, J., Qiu, S., and Wang, X. (2020). Heatwave-induced

human health risk assessment in megacities based on heat stress-social vulnerability-human exposure framework. Landsc. Urban Plann. *203*, 103907. https://doi.org/10.1016/j.landurbplan.2020.103907.
27. Butcher, S., Acuto, M., and Trundle, A. (2021). Leaving no urban citizens behind: An urban equality framework for deploying the sustainable development goals. One Earth *4*, 1548–1556. https://doi.org/10.1016/j.oneear.2021.10.015.
28. Khosla, R., Miranda, N.D., Trotter, P.A., Mazzone, A., Renaldi, R., McElroy, C., Cohen, F., Jani, A., Perera-Salazar, R., and McCulloch, M. (2020). Cooling for sustainable development. Nat. Sustain. *4*, 201–208. https://doi.org/10.1038/s41893-020-00627-w.
29. Jain, M., and Rohracher, H. (2022). Assessing transformative change of infrastructures in urban area redevelopments. Cities *124*, 103573. https://doi.org/10.1016/j.cities.2022.103573.
30. Oakes, T. (2019). Happy town: Cultural governance and biopolitical urbanism in China. Environ. Plan. A. *51*, 244–262. https://doi.org/10.1177/0308518X17693621.
31. Zheng, W., Shen, G.Q., Wang, H., Hong, J., and Li, Z. (2017). Decision support for sustainable urban renewal: A multi-scale model. Land Use Pol. *69*, 361–371. https://doi.org/10.1016/j.landusepol.2017.09.019.
32. Stewart, I.D., and Oke, T.R. (2012). Local Climate Zones for Urban Temperature Studies. Bull. Am. Meteorol. Soc. *93*, 1879–1900. https://doi.org/10.1175/BAMS-D-11-00019.1.
33. Shang, S., Du, S., Du, S., and Zhu, S. (2021). Estimating building-scale population using multi-source spatial data. Cities *111*, 103002. https://doi.org/10.1016/j.cities.2020.103002.
34. He, C., Ma, L., Zhou, L., Kan, H., Zhang, Y., Ma, W., and Chen, B. (2019). Exploring the mechanisms of heat wave vulnerability at the urban scale based on the application of big data and artificial societies. Environ. Int. *127*, 573–583. https://doi.org/10.1016/j.envint.2019.01.057.
35. Yuan, B., Zhou, L., Hu, F., and Zhang, Q. (2022). Diurnal dynamics of heat exposure in Xi'an: A perspective from local climate zone. Build. Environ. *222*, 109400. https://doi.org/10.1016/j.buildenv.2022.109400.
36. Zhou, Y., Zhang, G., Jiang, L., Chen, X., Xie, T., Wei, Y., Xu, L., Pan, Z., An, P., and Lun, F. (2021). Mapping local climate zones and their associated heat risk issues in Beijing: Based on open data. Sustain. Cities Soc. *74*, 103174. https://doi.org/10.1016/j.scs.2021.103174.
37. Chen, B., Xie, M., Feng, Q., Wu, R., and Jiang, L. (2022). Diurnal heat exposure risk mapping and related governance zoning: A case study of Beijing, China. Sustain. Cities Soc. *81*, 103831. https://doi.org/10.1016/j.scs.2022.103831.
38. Perera, N.G.R., and Emmanuel, R. (2018). A "Local Climate Zone" based approach to urban planning in Colombo, Sri Lanka. Urban Clim. *23*, 188–203. https://doi.org/10.1016/j.uclim.2016.11.006.
39. Zhou, W., Huang, G., and Cadenasso, M.L. (2011). Does spatial configuration matter? Understanding the effects of land cover pattern on land surface temperature in urban landscapes. Landsc. Urban Plann. *102*, 54–63. https://doi.org/10.1016/j.landurbplan.2011.03.009.
40. Wang, J., McPhearson, T., Zhou, W., Cook, E.M., Herreros-Cantis, P., and Liu, J. (2023). Comparing relationships between urban heat exposure, ecological structure, and socio-economic patterns in Beijing and New York City. Landsc. Urban Plann. *235*, 104750. https://doi.org/10.1016/j.landurbplan.2023.104750.
41. Xin, J., Yang, J., Jiang, Y., Shi, Z., Jin, C., Xiao, X., Xia, J.C., and Yang, R. (2023). Variations of Urban Thermal Risk with Local Climate Zones. Int. J. Environ. Res. Public Health *20*, 3283. https://doi.org/10.3390/ijerph20043283.
42. Jiang, S., Zhan, W., Dong, P., Wang, C., Li, J., Miao, S., Jiang, L., Du, H., and Wang, C. (2022). Surface air temperature differences of intra- and inter-local climate zones across diverse timescales and climates. Build. Environ. *222*, 109396. https://doi.org/10.1016/j.buildenv.2022.109396.
43. United Nations (2019). Nature-Based Solutions for Climate (UNEP - UN Environment Programme). http://www.unep.org/nature-based-solutions-climate.
44. Diep, L., and McPhearson, T. (2022). Nature-based solutions for global climate adaptation. Nature *606*, 653. https://doi.org/10.1038/d41586-022-01698-9.
45. UNEP (2021). Adaptation Gap Report 2020 (UNEP - UN Environment Programme). http://www.unep.org/resources/adaptation-gap-report-2020.
46. Geng, X., Yu, Z., Zhang, D., Li, C., Yuan, Y., and Wang, X. (2022). The influence of local background climate on the dominant factors and threshold-size of the cooling effect of urban parks. Sci. Total Environ. *823*, 153806. https://doi.org/10.1016/j.scitotenv.2022.153806.
47. Zhou, Y., Zhao, H., Mao, S., Zhang, G., Jin, Y., Luo, Y., Huo, W., Pan, Z., An, P., and Lun, F. (2022). Studies on urban park cooling effects and their driving factors in China: Considering 276 cities under different climate zones. Build. Environ. *222*, 109441. https://doi.org/10.1016/j.buildenv.2022.109441.
48. Yang, P., Xiao, Z.-N., and Ye, M.-S. (2016). Cooling effect of urban parks and their relationship with urban heat islands. Atmos. Ocean. Sci. Lett. *9*, 298–305. https://doi.org/10.1080/16742834.2016.1191316.
49. Yan, H., Wu, F., and Dong, L. (2018). Influence of a large urban park on the local urban thermal environment. Sci. Total Environ. *622–623*, 882–891. https://doi.org/10.1016/j.scitotenv.2017.11.327.
50. Dong, J., Lin, M., Zuo, J., Lin, T., Liu, J., Sun, C., and Luo, J. (2020). Quantitative study on the cooling effect of green roofs in a high-density urban Area—A case study of Xiamen, China. J. Clean. Prod. *255*, 120152. https://doi.org/10.1016/j.jclepro.2020.120152.
51. Zhang, B., Xie, G.D., Gao, J.X., and Yang, Y. (2014). The cooling effect of urban green spaces as a contribution to energy-saving and emission-reduction: A case study in Beijing, China. Build. Environ. *76*, 37–43. https://doi.org/10.1016/j.buildenv.2014.03.003.
52. Bartesaghi Koc, C., Osmond, P., and Peters, A. (2018). Evaluating the cooling effects of green infrastructure: A systematic review of methods, indicators and data sources. Sol. Energy *166*, 486–508. https://doi.org/10.1016/j.solener.2018.03.008.
53. Yang, J., Jin, S., Xiao, X., Jin, C., Xia, J.C., Li, X., and Wang, S. (2019). Local climate zone ventilation and urban land surface temperatures: Towards a performance-based and wind-sensitive planning proposal in megacities. Sustain. Cities Soc. *47*, 101487. https://doi.org/10.1016/j.scs.2019.101487.
54. Yang, J., Wang, Y., Xue, B., Li, Y., Xiao, X., Xia, J.C., and He, B. (2021). Contribution of urban ventilation to the thermal environment and urban energy demand: Different climate background perspectives. Sci. Total Environ. *795*, 148791. https://doi.org/10.1016/j.scitotenv.2021.148791.
55. Yang, J., Ren, J., Sun, D., Xiao, X., Xia, J.C., Jin, C., and Li, X. (2021). Understanding land surface temperature impact factors based on local climate zones. Sustain. Cities Soc. *69*, 102818. https://doi.org/10.1016/j.scs.2021.102818.
56. Li, N., Yang, J., Qiao, Z., Wang, Y., and Miao, S. (2021). Urban Thermal Characteristics of Local Climate Zones and Their Mitigation Measures across Cities in Different Climate Zones of China. Remote Sens *13*, 1468. https://doi.org/10.3390/rs13081468.
57. Yang, J., Wang, Y., Xiao, X., Jin, C., Xia, J.C., and Li, X. (2019). Spatial differentiation of urban wind and thermal environment in different grid sizes. Urban Clim. *28*, 100458. https://doi.org/10.1016/j.uclim.2019.100458.
58. Ren, J., Yang, J., Wu, F., Sun, W., Xiao, X., and Xia, J.C. (2023). Regional thermal environment changes: Integration of satellite data and land use/land cover. iScience *26*, 105820. https://doi.org/10.1016/j.isci.2022.105820.
59. Yang, J., Wang, Y., Xiu, C., Xiao, X., Xia, J., and Jin, C. (2020). Optimizing local climate zones to mitigate urban heat island effect in human settlements. J. Clean. Prod. *275*, 123767. https://doi.org/10.1016/j.jclepro.2020.123767.
60. Guo, A., Yang, J., Xiao, X., Xia, J.C., Jin, C., and Li, X. (2020). Influences of urban spatial form on urban heat island effects at the community level in China. Sustain. Cities Soc. *53*, 101972. https://doi.org/10.1016/j.scs.2019.101972.
61. Yang, J., Yang, Y., Sun, D., Jin, C., and Xiao, X. (2021). Influence of urban morphological characteristics on thermal environment. Sustain. Cities Soc. *72*, 103045. https://doi.org/10.1016/j.scs.2021.103045.
62. Allegra, M., and Maggor, E. (2022). The metropolitanization of Israel's settlement policy: The colonization of the West Bank as a strategy of spatial restructuring. Polit. Geogr. *92*, 102513. https://doi.org/10.1016/j.polgeo.2021.102513.
63. Tian, G., Qiao, Z., and Gao, X. (2014). Rural settlement land dynamic modes and policy implications in Beijing metropolitan region, China. Habitat Int. *44*, 237–246. https://doi.org/10.1016/j.habitatint.2014.06.010.
64. Demuzere, M., Kittner, J., Martilli, A., Mills, G., Moede, C., Stewart, I.D., van Vliet, J., and Bechtel, B. (2022). A global map of local climate zones to support earth system modelling and urban-scale environmental science. Earth Syst. Sci. Data *14*, 3835–3873. https://doi.org/10.5194/essd-14-3835-2022.
65. Tomlinson, C.J., Chapman, L., Thornes, J.E., and Baker, C.J. (2011). Including the urban heat island in spatial heat health risk assessment strategies: a case study for Birmingham, UK. Int. J. Health Geogr. *10*, 42. https://doi.org/10.1186/1476-072X-10-42.
66. Peng, J., Qiao, R., Liu, Y., Blaschke, T., Li, S., Wu, J., Xu, Z., and Liu, Q. (2020). A wavelet coherence approach to prioritizing influencing factors of land surface temperature and associated research scales. Rem. Sens. Environ. *246*, 111866. https://doi.org/10.1016/j.rse.2020.111866.

67. Kovats, R.S., and Hajat, S. (2008). Heat Stress and Public Health: A Critical Review. Annu. Rev. Public Health *29*, 41–55. https://doi.org/10.1146/annurev.publhealth.29.020907.090843.

68. Maggiotto, G., Miani, A., Rizzo, E., Castellone, M.D., and Piscitelli, P. (2021). Heat waves and adaptation strategies in a mediterranean urban context. Environ. Res. *197*, 111066. https://doi.org/10.1016/j.envres.2021.111066.

69. Meque, A., Pinto, I., Maúre, G., and Beleza, A. (2022). Understanding the variability of heatwave characteristics in southern Africa. Weather Clim. Extrem. *38*, 100498. https://doi.org/10.1016/j.wace.2022.100498.

70. Yu, Z., Yao, Y., Yang, G., Wang, X., and Vejre, H. (2019). Spatiotemporal patterns and characteristics of remotely sensed region heat islands during the rapid urbanization (1995–2015) of Southern China. Sci. Total Environ. *674*, 242–254. https://doi.org/10.1016/j.scitotenv.2019.04.088.

71. Buscail, C., Upegui, E., and Viel, J.-F. (2012). Mapping heatwave health risk at the community level for public health action. Int. J. Health Geogr. *11*, 38. https://doi.org/10.1186/1476-072X-11-38.

72. Chen, Q., Ding, M., Yang, X., Hu, K., and Qi, J. (2018). Spatially explicit assessment of heat health risk by using multi-sensor remote sensing images and socioeconomic data in Yangtze River Delta, China. Int. J. Health Geogr. *17*, 15. https://doi.org/10.1186/s12942-018-0135-y.

73. Li, L., and Zha, Y. (2020). Population exposure to extreme heat in China: Frequency, intensity, duration and temporal trends. Sustain. Cities Soc. *60*, 102282. https://doi.org/10.1016/j.scs.2020.102282.

74. Ma, L., Huang, G., Johnson, B.A., Chen, Z., Li, M., Yan, Z., Zhan, W., Lu, H., He, W., and Lian, D. (2023). Investigating urban heat-related health risks based on local climate zones: A case study of Changzhou in China. Sustain. Cities Soc. *91*, 104402. https://doi.org/10.1016/j.scs.2023.104402.

75. Zhang, R., Yang, J., Ma, X., Xiao, X., and Xia, J.C. (2023). Optimal allocation of local climate zones based on heat vulnerability perspective. Sustain. Cities Soc. *99*, 104981. https://doi.org/10.1016/j.scs.2023.104981.

76. Chen, J., Liu, Y., Pan, T., Ciais, P., Ma, T., Liu, Y., Yamazaki, D., Ge, Q., and Peñuelas, J. (2020). Global socioeconomic exposure of heat extremes under climate change. J. Clean. Prod. *277*, 123275. https://doi.org/10.1016/j.jclepro.2020.123275.

77. Amani-Beni, M., Chen, Y., Vasileva, M., Zhang, B., and Xie, G.D. (2022). Quantitative-spatial relationships between air and surface temperature, a proxy for microclimate studies in fine-scale intra-urban areas? Sustain. Cities Soc. *77*, 103584. https://doi.org/10.1016/j.scs.2021.103584.

78. Hrisko, J., Ramamurthy, P., Yu, Y., Yu, P., and Melecio-Vázquez, D. (2020). Urban air temperature model using GOES-16 LST and a diurnal regressive neural network algorithm. Rem. Sens. Environ. *237*, 111495. https://doi.org/10.1016/j.rse.2019.111495.

79. Guo, B., Bian, Y., Zhang, D., Su, Y., Wang, X., Zhang, B., Wang, Y., Chen, Q., Wu, Y., and Luo, P. (2021). Estimating Socio-Economic Parameters via Machine Learning Methods Using Luojia1-01 Nighttime Light Remotely Sensed Images at Multiple Scales of China in 2018. IEEE Access *9*, 34352–34365. https://doi.org/10.1109/ACCESS.2021.3059865.

80. Yazar, M., York, A., and Larson, K.L. (2022). Adaptation, exposure, and politics: Local extreme heat and global climate change risk perceptions in the phoenix metropolitan region, USA. Cities *127*, 103763. https://doi.org/10.1016/j.cities.2022.103763.

81. Ebert, U., and Welsch, H. (2004). Meaningful environmental indices: a social choice approach. J. Environ. Econ. Manag. *47*, 270–283. https://doi.org/10.1016/j.jeem.2003.09.001.

82. Peng, J., Liu, Y., Li, T., and Wu, J. (2017). Regional ecosystem health response to rural land use change: A case study in Lijiang City, China. Ecol. Indicat. *72*, 399–410. https://doi.org/10.1016/j.ecolind.2016.08.024.

83. Suo, A.-N., Xiong, Y.-C., Wang, T.-M., Yue, D.-X., and Ge, J.-P. (2008). Ecosystem Health Assessment of the Jinghe River Watershed on the Huangtu Plateau. EcoHealth *5*, 127–136. https://doi.org/10.1007/s10393-008-0167-z.

84. Ramsay, Emma, E., Genie, M., Fleming, Peter, A., Faber, S., Fiona, Barker, Rohan Sweeney, Ruzka, R., Taruc, Steven L., Chown, Grant, A., and Duffy. (2021). Chronic heat stress in tropical urban informal settlements. *Iscience 24*, 11.

85. Simpson, N.P., Williams, P.A., Mach, K.J., Berrang-Ford, L., Biesbroek, R., Haasnoot, M., Segnon, A.C., Campbell, D., Musah-Surugu, J.I., Joe, E.T., et al. (2023). Adaptation to compound climate risks: A systematic global stocktake. Iscience *26*, 105926.

86. Yoo, C., Im, J., Weng, Q., Cho, D., Kang, E., and Shin, Y. (2023). Diurnal urban heat risk assessment using extreme air temperatures and real-time population data in Seoul. Iscience *26*, 108123.

87. Shen, Pengke, and Shuqing, Zhao (2024). Intensifying urban imprint on land surface warming: insights from local to global scale. iScience *27*, 109110.

STAR★METHODS

KEY RESOURCES TABLE

REAGENT or RESOURCE	SOURCE	IDENTIFIER
Deposited data		
Daily maximum temperature	RP5	rp5.ru/
Global population distribution raster	Oak Ridge National Laboratory	landscan.ornl.gov/
Daily MODIS land surface temperature(MOD11A1)	US Geological Survey (USGS)	https://doi.org/10.5067/MODIS/MOD11A1.061
16-d enhanced vegetation index(MOD13A2)	US Geological Survey (USGS)	https://doi.org/10.5067/MODIS/MOD13A2.061
POI data	Open street map	www.openstreetmap.org/
Road data	Open street map	www.openstreetmap.org/
LCZ maps	Demuzere et al.[64]	https://zenodo.org/records/6364594
Night time night(VIIRS)	US Geological Survey (USGS)	https://developers.google.com/earth-engine/datasets/catalog/NOAA_VIIRS_DNB_ANNUAL_V21
Software and algorithms		
ArcGIS Pro 3.1	ESRI	www.arcgis.com

RESOURCE AVAILABILITY

Lead contact

Further information and requests for resources should be directed to and will be fulfilled by the lead contact, Jun Yang (yangjun8@mail.neu.edu.cn).

Materials availability

This study did not generate new unique materials.

Data and code availability

- Data: All statistical data reported in this paper will be shared by the lead contact upon request. Daily maximum temperature data were deposited at rp5.ru/; population spatial distribution data were deposited at landscan.ornl.gov/; land surface temperature, enhanced vegetation index, and nighttime lighting are derived from US Geological Surve and can be accessed, respectively, at https://doi.org/10.5067/MODIS/MOD11A1.061, https://doi.org/10.5067/MODIS/MOD13A2.061, https://developers.google.com/earth-engine/datasets/catalog/NOAA_VIIRS_DNB_ANNUAL_V21; POI and road data from Open street map, available at www.openstreetmap.org/; LCZ maps from Demuzere et al.,[64] deposited at https://zenodo.org/records/6364594.
- Code: This paper does not report the original code.
- Any additional information required to reanalyze the data reported in this paper is available from the lead contact upon request.

EXPERIMENTAL MODEL AND STUDY PARTICIPANT DETAILS

This study did not involve experimental models or study participants.

METHOD DETAILS

Study area

We initially selected study areas based on broad geographic divisions within developing countries. Four metropolitan areas were selected from East Asia, South Asia, Southeast Asia, and the Middle East, along with one study area each from Africa and Latin America. Further, we established specific criteria for selecting study areas, including (1) a population exceeding 10 million people; (2) a region with notable high temperatures; and (3) an area greater than 2,000 square kilometers to ensure the significance of the study results.

Under these criteria, we excluded metropolitan areas such as Cape Town, South Africa, and Caracas, Venezuela, because of lower population exposure (under criteria 1); we chose Beijing, China, over Shanghai, China, because of its more pronounced extreme summer heat (under criteria 2), and Rio de Janeiro, Brazil, out of São Paulo and Rio de Janeiro, Brazil, because of its year-round high temperatures; and we excluded metropolitan areas such as Mexico City, Mexico, and Nairobi, Kenya, owing to their small size (under criteria 3). Therefore,

we chose the following metropolitan areas in developing countries: Beijing, China; Cairo, Egypt; Mumbai, India; Jakarta, Indonesia; Tehran, Iran; and Rio de Janeiro, Brazil (the global distribution of the study area is shown in Figure 6).

According to demographic data provided by Oak Labs, these metropolitan areas all had a population exceeding 10 million people by the end of 2020, with a total combined population of 118.5 million people. These areas are all located in low- and mid-latitudes. According to Moderate Resolution Imaging Spectroradiometer (MODIS) land surface temperature data, their mean maximum temperature was above 49°C between 2018 and 2022, with over 100 recorded extreme heat events during this period.

The distribution and composition of LCZ landscapes in each metropolitan area are visually presented in Figure S1. The spatial distribution of LCZ exhibits a discernible clustering pattern. Within the urbanized regions of these metropolitan areas, the primary built-up landscape types encompass LCZ 1-5, with LCZ 8, LCZ 6, LCZ 9, and LCZ A-G extending progressively outward. The proportion of mid-rise (LCZ 1-2, 4-5) landscapes in the built-up areas remains below 15% across all metropolitan areas. Notably, the Beijing metropolitan area exhibits a significantly higher prevalence of high-rise built landscapes compared to the other metropolitan areas. Conversely, the Cairo metropolitan area records a complete absence of high-rise built landscapes, while the Tehran metropolitan area boasts the highest proportion of mid-rise built-up landscapes among the metropolitan areas. Low-rise landscapes (LCZ 3, 6, 8, 9) constitute over 75% of the total landscape composition in all metropolitan areas. LCZ 3, LCZ 8, and LCZ 9 typically account for more than 10% of the built landscape type in each metropolitan area. Turning to the natural landscape types, Cairo and Tehran exhibit the highest proportion of LCZ F, characterized by bare ground. On the other hand, Beijing, Jakarta, Rio de Janeiro, and Mumbai showcase the highest proportion of LCZ A, characterized by dense trees. LCZ D, representing low vegetation, surpasses the 10% mark in each metropolitan area and holds significant importance within the natural landscape types.

Data

We used meteorological, demographic, remote sensing, points of interest, road network, and LCZ data, as shown in key resources table. Meteorological data used to determine the timing of heat waves were obtained from rp5.ru. The remote sensing data included MODIS land surface temperature products, MODIS enhanced vegetation index products, and National Oceanic and Atmospheric Administration (NOAA) nighttime light VIIRS products provided by the US Geological Survey (USGS) and downloaded from the Google Earth engine hosting server. Population data were obtained from the LandScan global population map released by the Oak Ridge National Laboratory. The POI and road network data were obtained from Open Street Map. Urban landscape data originated from the official global LCZ map released by the World Urban Database and Access Portal Tools, the largest open-source LCZ mapping community.[64]

HHR assessment

Our HHR assessment methodology was based on an in-depth understanding of the IPCC Framework for Climate-Environmental Risk Assessment, a comprehensive review of previous HHR studies, and the availability of global data. The IPCC Working Group II proposed a risk-centered assessment framework in its Fifth[7] and Sixth Assessment Reports,[1] reflecting the well-known Crichton Risk Triangle.[65] In this framework, risk is described as a function of hazard, human exposure, and vulnerability. Hazard refers to "a natural or human-induced physical event or trend or the potential occurrence of physical impacts that may result in loss of life, injury or other health impacts, as well as damage to and loss of property, infrastructure, livelihoods, service delivery, ecosystems, and environmental resources." Exposure refers to "the presence of people, livelihoods, species or ecosystems, environmental functions, services and resources, infrastructure or economic, social or cultural assets in places and environments where they may be adversely affected." Vulnerability refers to "the tendency or disposition to be adversely affected [and] encompasses a variety of concepts and elements, including sensitivity or susceptibility to harm and a lack of coping and adaptive capacity."

According to previous studies, a 1-km scale grid demonstrates the highest wavelet coherence between urban surface temperature and subsurface factors.[66] Therefore, we assessed HHR levels according to heat hazard, exposure, and vulnerability on a 1-km scale grid using ArcGIS Pro 3.1. The specific assessment methods for heat hazard, heat exposure, and heat vulnerability are shown below.

Heat hazard

"Hazard refers to a natural or human-induced physical event or trend, or the potential manifestation of such events, which may lead to the loss of life, injury, or other health-related impacts."[1] Within this study, the degree of heat hazard is conceptualized as the potential harm that humans may face due to elevated temperatures during a heat wave. The precise definition of a heat wave and the categorization of hazard levels play a pivotal role in assessing the extent of risk.

Heat waves are characterized as prolonged periods of excessively high temperatures. While there is no universally accepted global standard for defining heat waves, they can generally be categorized into two main types: absolute and relative definitions. Absolute heat wave definitions rely on officially established temperature thresholds set by governmental bodies and are commonly employed in studies focused on specific regions. On the other hand, relative heat wave definitions acknowledge the substantial variations in the capacity of populations across different regions to endure high temperatures due to physiological, behavioral, and cultural factors. As a result, criteria for relative heat waves cannot be uniformly applied, as they require consideration of these contextual differences.[67] The heat wave definition adopted in this study follows the guidelines set forth by the World Meteorological Organization (WMO). According to the WMO, a heat wave is characterized by a period of time during which the daily maximum temperature surpasses the average maximum temperature by more than 5 degrees Celsius and persists for a duration exceeding 5 days.[68]

However, it is worth noting that in many contemporary studies, an alternative approach is employed, wherein a heat wave is defined as a period of multiple consecutive days with temperatures exceeding 90% of the highest temperature recorded at the specific location within a year.[69,70] Considering the diverse climatic conditions across different study areas, this relative definition method has been employed in the present study to define heat waves as weather phenomena with maximum temperatures surpassing 90% of the local annual threshold for three consecutive days. Figure S2 illustrates the temperature patterns observed in each metropolitan area throughout the year 2020. The identified heat wave periods for each metropolitan area are as follows: Beijing experienced a heat wave from August 2nd to August 4th, Cairo from May 19th to May 21st, Jakarta from June 29th to July 1st, Mumbai from December 7th to December 9th, Rio de Janeiro from February 18th to February 20th, and Tehran from July 27th to July 29th.

Enhancements in the availability and accessibility of remotely sensed thermal data represent a significant technological advancement. Across the majority of the reviewed articles, surface temperature data have emerged as a valuable alternative for exploring thermal health risks and vulnerabilities in urban areas and cities, particularly in developing regions where air temperature data are limited .[18,19,34–36,71–75] To provide a more detailed understanding of the spatial distribution of heat hazards within each metropolitan area, this study utilized MODIS LST (Land Surface Temperature) products during identified heat wave periods. While acknowledging that LST may not entirely capture residents' actual temperature perception, numerous studies have shown a strong correlation between LST and air temperature. Furthermore, while some studies rely on coarse-grained weather station data or climate reanalysis data, these datasets do not meet the specific needs of this paper at the one-kilometer scale.[20,26,76] LST offers a higher spatial resolution, making it well-suited for grid-scale analyses and applications. Therefore, despite its limitations, LST was chosen as a suitable proxy for temperature in this study to enable a more refined characterization of the spatial variability of heat hazards in the metropolitan areas.[77,78] The processing method for MODIS LST products is shown in Equation 1.

$$LST = DN \times 0.02 - 273.15, \quad \text{(Equation 1)}$$

where, LST represents the surface temperature measured in degrees Celsius, while DN refers to the brightness value of the image element. As the temperature rises, so does the potential heat hazard to the human body. Therefore, the LST values undergo positive normalization to ensure an accurate reflection of this relationship.

Heat exposure

"Exposure entails the presence of individuals, livelihoods, species, ecosystems, environmental functions, services, resources, infrastructure, or economic, social, and cultural assets in areas and environments where they may encounter adverse impacts".[1] In the context of this study, heat exposure refers to the potential impact on individuals within a designated grid area due to prevailing heat conditions. Typically, a higher concentration of individuals within a grid correlates with elevated levels of heat exposure.

In the majority of the reviewed literature, assessments of heat-related health risks relied on population density metrics, including the utilization of census data from administrative districts[19,20,26,71] or the application of spatially downscaled data generated from supplementary sources such as points of interest (POIs), nighttime lighting, etc.[18,34,36,72,74] This study employed Landscan Global population data at the grid scale, obtained from the Oak Ridge National Laboratory in the United States, as a spatial proxy for population density. LandScan Global, an innovative product resulting from the integration of geospatial science, remote sensing technology, and machine learning algorithms, represents the highest resolution global population distribution data, depicting ambient (24-hour average) population distributions. Given the diverse spatial data availability, quality, scale, accuracy, and cultural settlement practices across different regions, the LandScan population distribution model has been tailored to match the specific data conditions and geographic characteristics of each country and region. By capturing the surrounding population, LandScan Global encompasses all potential areas where people are active throughout the day and night, rather than solely residential zones. Consequently, it facilitates various applications such as emergency preparedness, risk assessments, site suitability studies, and other endeavors reliant on precise population data.With a spatial resolution of 1 km globally, the LandScan Global data aligns seamlessly with the spatial scale of Land Surface Temperature (LST), ensuring high accuracy in analyses and applications.

Figure S3 illustrates the spatial distribution of population within each metropolitan area, specifically highlighting the population carried by different types of built-up areas. It is observed that compact landscapes tend to accommodate larger populations compared to open landscapes of similar characteristics. For instance, in the Beijing metropolitan area, the population density follows the order of high-rise buildings > mid-rise buildings > low-rise buildings. In the Cairo, Mumbai, and Tehran metropolitan areas, the highest population concentration is observed in the mid-rise landscape. On the other hand, the compact high-rise landscapes in the Jakarta and Rio metropolitan areas exhibit relatively lower population densities.

Heat vulnerability

"Vulnerability entails the tendency or disposition to be adversely affected [and] encompasses a variety of concepts and elements, including sensitivity or susceptibility to harm and a lack of coping and adaptive capacity". In this study, heat vulnerability is characterized as the susceptibility to harm and the capacity to adapt when both humans and infrastructure within the grid are negatively impacted by the thermal environment. In general, socio-economic status and age structure are considered to be sensitivity factors, while natural and socio-economic resources are considered to be capability factors.[19]

In terms of sensitivity factors, there exists a negative correlation between lower socio-economic status and increased heat-related mortality. Previous research has illustrated a positive association between night-time lighting, road density, and socio-economic conditions.[79]

Consequently, despite the weak correlation with income levels, data on road density and night-time lighting were utilized as indirect indicators for socio-economic variables. Elderly individuals and young children exhibit heightened sensitivity to heat-related health risks due to their physiological vulnerabilities and reduced tolerance to elevated temperatures. However, the assessment system does not incorporate age structure due to the heterogeneous nature of available global age structure data, which is primarily available at the administrative district scale. This results in grids within the same district sharing identical age structures, which contradicts the grid-scale assessment objective of this study.

For adaptive factors, abundant vegetation is frequently linked with decreased heat-related mortality, as it can mitigate high temperatures by absorbing heat. MODIS EVI (Enhanced Vegetation Index) serves as a localized measure of vegetation abundance and thus serves as an indicator of vulnerability. Furthermore, general hospitals and community health facilities are pivotal in preserving population health as vital social resources in combating diseases. Consequently, this study utilizes the distance from health facilities as one of the adaptation indicators.

In summary, to assess the heat vulnerability of the grid, four indicators are employed:

(1) Road density surrounding the grid (RD): The density of road networks surrounding the grid serves as an indicator of local socioeconomic conditions. Areas with a higher density of roads generally indicate greater socioeconomic development and improved access to medical resources, thereby enhancing resilience and adaptability to heat-related health risks.[34] Therefore, this study obtains the road density by performing line density analysis on the road data provided by the Open street map. The road network density RD is calculated as shown in Equation 2

$$RD = \sum_{i=1}^{n} L_i \Big/ \pi r^2, \quad \text{(Equation 2)}$$

where, r denotes the search radius, πr^2 denotes the area of a circular search region. L_i denotes the length of the i-th road intercepted in the search region, and $\sum_{i=1}^{n} L_i$ denotes the length and of all intercepted roads in the search region.

(2) Nighttime light index (NTL): The nighttime light index is another measure that reflects the level of socioeconomic development within the grid. Areas with higher levels of socioeconomic development are generally more resilient to heat-related health risks.[18] In this study, the Visible infrared Imaging Radiometer (VIIRS) nighttime light images were resampled to a 1 km resolution to serve as an element for assessing heat health risks.

(3) The minimum Euclidean distance between the grid and medical aid institutions (DH): The proximity of the grid to medical aid institutions plays a crucial role in ensuring timely treatment during heat stress incidents. In this study, cost path analysis was conducted on hospital points of interest (POI) data obtained from OpenStreetMap to determine the distance between the grid and the nearest medical aid institution. DH_i represents the Euclidean distance between the grid and the i-th medical aid institution, which can be expressed as Equation 3.

$$DH_i = \sqrt{(x - x_i)^2 + (y - y_i)^2}, \quad \text{(Equation 3)}$$

where, x and y represent the longitude and latitude coordinates of the grid, x_i. y_i represent the longitude and latitude coordinates of the i-th medical assistance institution.

DH represents the shortest Euclidean distance between the grid and medical aid institutions. If there are n medical aid institutions in the research area, then

$$DH = \min(DH_1, DH_2, \ldots, DH_n) \quad \text{(Equation 4)}$$

(4) Enhanced Vegetation Index (EVI): Urban green spaces have the potential to offer shade to pedestrians and effectively alleviate the impacts of extreme heat and heat island effects.[72,80] In this study, the MODIS EVI serves as an indicator of the vegetation coverage within the grid, thus reflecting the grid's sensitivity to heat-related health risks. EVI can be expressed in Equation 5.

$$EVI = \frac{2.5(nir - red)}{(nir + 6 * red - 7.5 * blue + 1)}, \quad \text{(Equation 5)}$$

In the formula, *nir*, *red*, *blue* represent the near-infrared band, red band and blue band of MODIS image respectively.

Among the aforementioned indicators, DH is considered a positive indicator of heat health risk, whereas RD, NTL, and EVI are regarded as negative indicators. To address multicollinearity among these heat vulnerability indicators, each indicator was separately normalized. The principal component analysis (PCA) tool in ArcGIS Pro 3.1 was then employed to synthesize these indicators and generate a comprehensive heat vulnerability measure.

Principal component analysis is a statistical technique that transforms a set of vectors into multiple orthogonal bases. This transformation ensures that the covariance between any two fields becomes zero, while maximizing the variance of the fields. By applying PCA, the original data is projected onto these orthogonal bases, enabling a more comprehensive and meaningful representation of the heat vulnerability factors.

The four vulnerability indicators were zero-averaged to form a matrix M by row.

$$M = \begin{pmatrix} RD_1 & \cdots & RD_i \\ \vdots & \ddots & \vdots \\ EVI_1 & \cdots & EVI_i \end{pmatrix}, \quad \text{(Equation 6)}$$

The covariance matrix C is a symmetric matrix , meaning that its elements are symmetrically positioned along the main diagonal. The diagonal elements represent the variances of each individual field, while the off-diagonal elements represent the covariances between the two fields. This symmetric arrangement reflects the relationship between the variables and provides valuable information about their statistical dependencies.

$$C = \frac{1}{m} MM^T, \quad \text{(Equation 7)}$$

Find all eigenvalues λ of the covariance matrix and the corresponding eigenvectors PC.Then the vulnerability can be expressed as:

$$\text{vulnerability} = \text{Nor}(\lambda_1 PC_1 + \lambda_2 PC_2 + \lambda_3 PC_3 + \lambda_4 PC_4), \quad \text{(Equation 8)}$$

where, Nor() denotes the normalization process. Since vulnerability consists of four indicators, four principal components can be generated. Use λ_i and PC_i to denote the ith eigenvalue and eigenvector, respectively.

The solution of the grid-scale

We standardized the scale of Heat Health Risk (HHR) assessment to 1000 meters, encompassing six parameters. Among these, the land surface temperature data provided by MODIS and the population data from Landscan Global are inherently at a 1000-meter scale and thus require no adjustment. The resolution of VIIRS nighttime light data and MODIS EVI data is originally at 500 meters and 250 meters, respectively, necessitating adjustment to fit the 1000-meter scale. To achieve this, we utilized mean resampling in ArcGIS Pro 3.1.The parameters of distance from hospitals and road density were derived from vector data obtained from OpenStreetMap, employing spatial analysis tools in ArcGIS Pro 3.1. In configuring the hyperparameters, we set the output resolution to 1000 meters to maintain consistency with the HHR evaluation scale.Furthermore, throughout the production process of the six HHR evaluation elements, we configured the capture grid option in the ArcGIS Pro geographic analysis environment to align the grid of all HHR evaluation elements with the population data grid provided by Landscan Global.

Synthesis of HHR

HHR was generated based on the principle of addition or multiplication. The formation of human health risks caused by heat waves is complex and primarily influenced by the physical climate system, socioeconomic conditions, and human perceptions. We applied the law of multiplication to the synthesis of hazard, exposure, and vulnerability. In principle, Ebert and Welsch analyzed both additive and multiplicative aggregations in relation to a specific validity criterion, namely that the resulting index should yield identical rankings when different normalizations or standardizations are used. They found that multiplicative aggregations have better validity than additive aggregations and better reflect synergetic processes between indicators.[81] In contrast, a weighted linear summation between indicators is subjective and does not reflect the complexity of HHR formation.[26] In practical application, Dong used the multiplicative principle to calculate the human health risk due to a heat wave.[6] Target layer aggregation based on the multiplicative principle has also been widely used in other ecosystem health assessments.[82,83] Therefore, we applied the multiplicative method for the synthesis of indicators; the HHR level can be expressed by Equation 9:

$$HHR = \sqrt[3]{h * e * v} \quad \text{(Equation 9)}$$

where h, e, and v denote the normalized heat hazard, exposure, and vulnerability degrees, respectively.

To further describe the causes of HHR, we referred to the approach described by Dong et al. to classify h, e, and v into high and low (H and L) categories, thus generating eight specific HHR types: Hh-He-Hv, Lh-He-Hv, Hh-Le-Hv, Hh-He-Lv, Lh-Le-Hv, Hh-Le-Lv, Lh-He-Lv, and Lh-Le-Lv.[26] The natural breakpoint method was used for high and low classification. Natural breakpoints are located by minimizing the within-group variance and maximizing the between-group variance, ensuring that it more accurately captures the inherent patterns and variations in the data while reducing the subjectivity of the classification thresholds. In addition, the principles of the natural breakpoint method make it sensitive to changes in data patterns and, thus, more suitable for application to the complex and non-linearly distributed datasets in this study. Most of the literature reviewed thus far applies the natural breakpoint method for grading HHR;[9,18,74,75] therefore, we concluded that it is reasonable to use the natural breakpoint method to grade h, e, and v.

Impact of local landscape composition on the HHR level

HHR assessment had a 1-km spatial scale, while LCZ maps had a spatial resolution of 100 m. Therefore, after spatial resampling, each HHR assessment unit contained 10 × 10 landscape units. In this study, the LCZ type with the highest proportion within the grid was considered the dominant type[84–87].

Using SPSS 26, we developed a stepwise linear regression model to analyze the correlation between local LCZ composition (based on the dominant built LCZ type) and HHR level, distinguishing the differential effects of landscape composition in urban, suburban, and peripheral areas.

Stepwise linear regression enabled the selection of the most important variables and analysis of specific correlations between the explanatory variable (LCZ composition) and predictor variable (HHR level). The model tested the significance and contribution of each variable by separately introducing explanatory variables and removing variables that did not meet the criteria. At $p < 0.10$, the explanatory variable remained in the model, whereas at $p \geq 0.10$, the explanatory variable was removed; this process was repeated until no explanatory variables were added or removed. The regression model is depicted in Equation 10:

$$HHR = \beta_1 \times LCZX_1 + \beta_2 \times LCZX_2 + \cdots + \beta_n \times LCZX_n + b \quad \text{(Equation 10)}$$

where, $LCZX_n$ denotes the proportion of the n^{th} LCZ in the grid, β_n denotes the influence of $LCZX_n$ on the HHR level, and b is a constant.

QUANTIFICATION AND STATISTICAL ANALYSIS

Statistical methods have been indicated in the corresponding figures. A two-tailed $p < 0.10$ was considered to indicate statistical significance in the stepwise linear regression model. All statistical analyses were performed using Origin 2021 and SPSS 26.